



# Magnetization reversal in nanotriangles fabricated by nanosphere lithography

X.H. Wang, M. Chandra Sekhar, I. Purnama, W.S. Lew<sup>\*</sup>, S. Goolaup, C.X. Cong

School of Physical and Mathematical Sciences, Nanyang Technological University, 21 Nanyang Link 637371, Singapore

## ARTICLE INFO

### Article history:

Received 17 June 2011

Received in revised form 13 June 2012

Accepted 14 June 2012

Available online 21 June 2012

### Keywords:

Nanosphere lithography

Magnetic nanostructures

Magnetization reversal

Magnetic property simulation

## ABSTRACT

We report on the magnetization reversal behavior of sub 100-nm triangular shaped  $\text{Ni}_{80}\text{Fe}_{20}$  dot array fabricated by nanosphere lithography. Hysteresis loops measured by magneto-optical Kerr effect magnetometry are classified into single and double-switched loops in 45 nm, 80 nm and 100 nm triangular nanomagnets. Micromagnetic simulations show that a plateau observed in the double-switched loop in the 100-nm triangular nanomagnet is due to the formation of a metastable mediating V state.

© 2012 Elsevier B.V. All rights reserved.

## 1. Introduction

Towards delaying the onset of thermal effect and superparamagnetic limit in the ultrahigh density recording media, patterned magnetic thin film nanostructures have been proposed [1,2]. For optimum performance of the patterned storage medium, understanding and controlling the magnetic properties of individual and interacting nanomagnets are of key importance. Variations of patterned magnetic nanostructures such as rectangles [3], dots [4], triangles [5], and rings [6] have been extensively studied. The magnetization reversal mechanisms in patterned magnetic structures are determined by the competition of magnetic energy terms, *i.e.* magnetostatic, exchange, anisotropy, and Zeeman energy. By tailoring the shape of the patterns, the magnetization reversal process can be engineered. Thus, fabricating designed patterns with high resolution is important. Conventional lithography techniques, such as electron beam lithography [7], interference lithography [8], and X-ray lithography, have enabled large scale nanopattern fabrication. However, the resolution of the conventional lithography is dependent on the ratio of  $\lambda/\text{NA}$ , where  $\lambda$  is the wavelength, and NA is the numerical aperture (NA) of the system, and thus it is limited by the light-source device. From application viewpoint, a lithographic process that can pattern thin films into nanoscale patterns at an economically acceptable cost is vital. Non-wavelength nanofabrication approach technologies have been proposed to prepare large-area 2D or 3D colloidal pattern surfaces, such as self-assembly, electric-field-induced electrokinetic flowing, and Langmuir–Blodgett deposition [9–12]. Nanosphere lithography (NSL) is a non-conventional lithography that makes use of self-assembly of nanospheres to fabricate nanostructure and nanostructure arrays. A number of nanostructure shapes, such as triangular, hexagonal, ring

[13] and chains have been fabricated by using different techniques through NSL.

In this work, we have studied the magnetization reversal process in nanoscale triangular dots fabricated by NSL. Triangular shaped nanomagnets with different lateral sizes were patterned over an area of  $30\ \mu\text{m}^2$ . The hysteresis behavior of the nanomagnets was characterized using magneto optical Kerr effect (MOKE) techniques. Magnetic force microscopy (MFM) scanning was employed to observe the magnetic configurations. Our measurement results reveal that the magnetic hysteresis properties of the triangular nanomagnets are markedly sensitive to the lateral dimensions of the structures. Micromagnetic simulations were carried out to confirm the experimental results.

## 2. Methods

Monodispersed nanospheres with diameters of 465 nm, 365 nm and 200 nm were diluted into water with 2.6%wt. The solutions were further mixed by an equal amount of ethanol. About  $5\ \mu\text{l}$  of the prepared solutions (mixture of ethanol and polystyrene (PS) solution with volume ratio of 1:1) was dropped onto the surface of a  $3\ \text{cm} \times 3\ \text{cm}$  large clean silicon wafer. The silicon wafer was kept in 10% dodecylsulfate solution for 12 h previously. The wafer was then slowly immersed in deionized water after which a monolayer of PS spheres started to form on the water surface. The monolayer was lifted off from the water surface by using another cleaned Si wafer. The Si wafer (with PS spheres on top of it) is dried in air at room temperature.

The fabricated monolayer nanosphere arrays were then used as templates to create magnetic patterns. 15-nm-thick  $\text{Ni}_{80}\text{Fe}_{20}$  layer was deposited on the templates using electron beam evaporation technique. The deposition pressure was maintained at  $2.66 \times 10^{-4}$  Pa, while the

<sup>\*</sup> Corresponding author. Tel.: +65 63162963.

E-mail address: [wensiang@ntu.edu.sg](mailto:wensiang@ntu.edu.sg) (W.S. Lew).

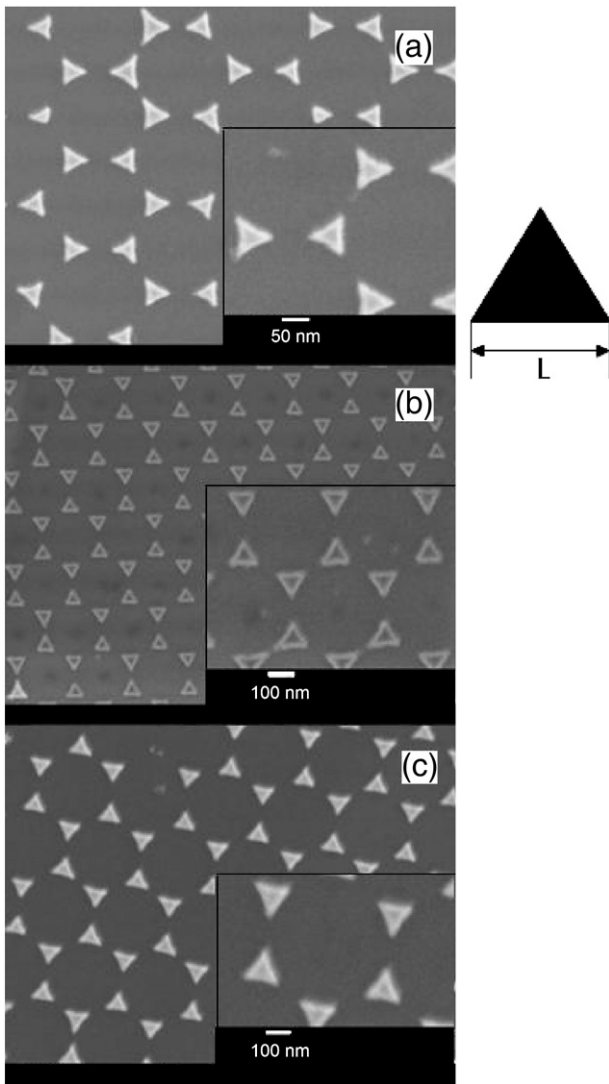


**Fig. 1.** Scanning electron micrograph of NiFe dot arrays fabricated by NSL with the feature of about 45 nm, 80 nm and 100 nm. The respective insets show the close-up image of the nanotriangles.

growth rate was kept at 2 Å/s. After the deposition, the nanospheres were lifted-off by immersing the template in a  $\text{CHCl}_3$  solution, assisted by ultrasonic agitation. The formation of the triangular nanomagnets is confirmed by scanning electron microscope (SEM) imaging at 10 kV operating voltage. Shown in Fig. 1 are the SEM images of the triangular nanomagnets of different lateral dimensions. The SEM image shows that the nanomagnets are equilateral and have uniform shape and size over a large area. Using PS nanospheres of different sizes

(465 nm–200 nm), equilateral nano-triangles of lateral sizes of 100 nm, 80 nm, and 45 nm were obtained. We have made the histograms of the nanotriangles and results are plotted in Fig. 2. The standard deviations are found to be 12.5 nm, 7.5 nm and 10.5 nm for 100 nm, 80 nm and 45 nm nanotriangles respectively. The area comprised by uniformly distributed triangles with no connecting film is found to be of 20–30  $\mu\text{m}$ , which is close to the size of the beam spot in our focused longitudinal MOKE measurement ( $\sim 30 \mu\text{m}$ ). All the measurements were carried out at room temperature.

### 3. Results and discussions

Shown in Fig. 3 are the typical MOKE hysteresis loops (a, b and c) for the 15-nm-thick NiFe triangular nanostructures of different lateral sizes ( $L$ ). During the measurements, an in-plane magnetic field was applied along the base direction of the nanotriangles. The open symbols represent the magnetic signal from the nanotriangles. The magnetization loops of the triangular nanomagnets are markedly sensitive to the lateral dimensions. As shown in Fig. 3(a), several features are observed in the hysteresis loop for  $L = 100$  nm. When the field is reversed from negative to positive direction, a two-step magnetization switching was observed. The first magnetization switching occurs at a low field of around +1.6 kA/m, resulting in a plateau with a field range ( $\Delta H_x$ ) of around 4 kA/m. The presence of the plateau indicates the formation of an intermediate state during the switching process. Further increasing the field along the positive direction, a major jump in magnetization is observed which leads to reverse saturation. The coercivity of the 100 nm triangle is found to be 9 kA/m. When the lateral dimension is reduced to 80 nm, the hysteresis loop shows a single switching behavior as shown in Fig. 3(b), it is a characteristic of coherent switching process where the magnetization reverses without any intermediate state. The measured coercivity is found to be increased to 9.6 kA/m. When  $L$  is further reduced to 45 nm, a nearly rectangular-shaped hysteresis loop is observed. However, the coercivity is observed to be increased further to 16 kA/m, as shown in Fig. 3(c). The signal-to-noise ratio is relatively low due to the small magnetic volume. The significant increase in the coercivity of the nano-triangle arrays as the dimensions are reduced is attributed to the change in the reversal mechanism and the increased stability of the remanent state.

In order to obtain a better understanding of the reversal process in the different triangular nanomagnets, we used the OOMMF code [14] to carry out the micromagnetic simulations. The parameters used in the simulations are saturation magnetization  $M_s = 860 \times 10^5$  A/m, exchange stiffness constant  $A = 1.3 \times 10^{-11}$  J/m, anisotropy constant  $K = 0$  J/m<sup>3</sup>, and chosen cell size is 2 nm. The simulated hysteresis loops for dimensions corresponding to Fig. 3(a), (b), and (c) are shown in Fig. 3(a'), 3(b') and 3(c'), respectively. The shape of the measured MOKE hysteresis loop is well reproduced by the simulation. For  $L = 100$  nm nanotriangles, a two-step hysteresis loop is obtained which confirms the intermediate state in the reversal process. The nanotriangles with lateral dimensions 80 nm and 45 nm are characterized by a single switching process,

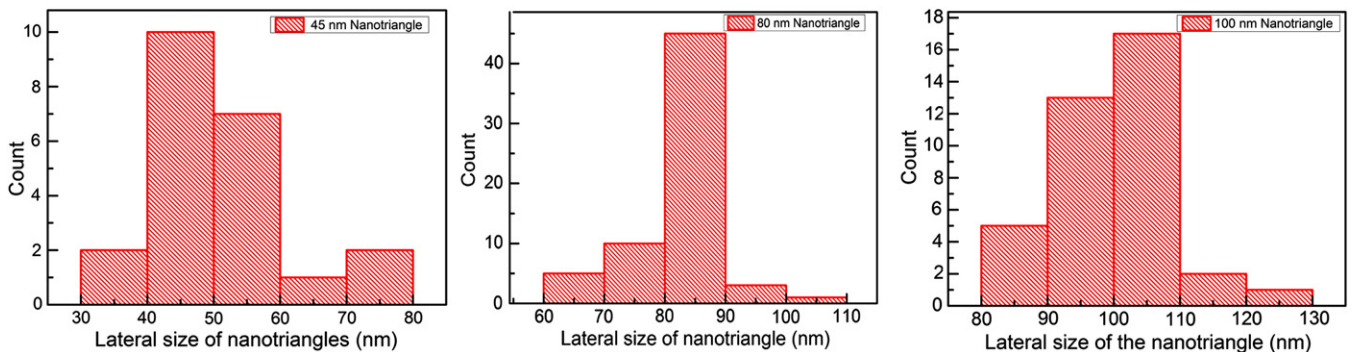


**Fig. 2.** The histograms of the nanotriangle areas for different dimensions: 45 nm, 80 nm, and 100 nm.

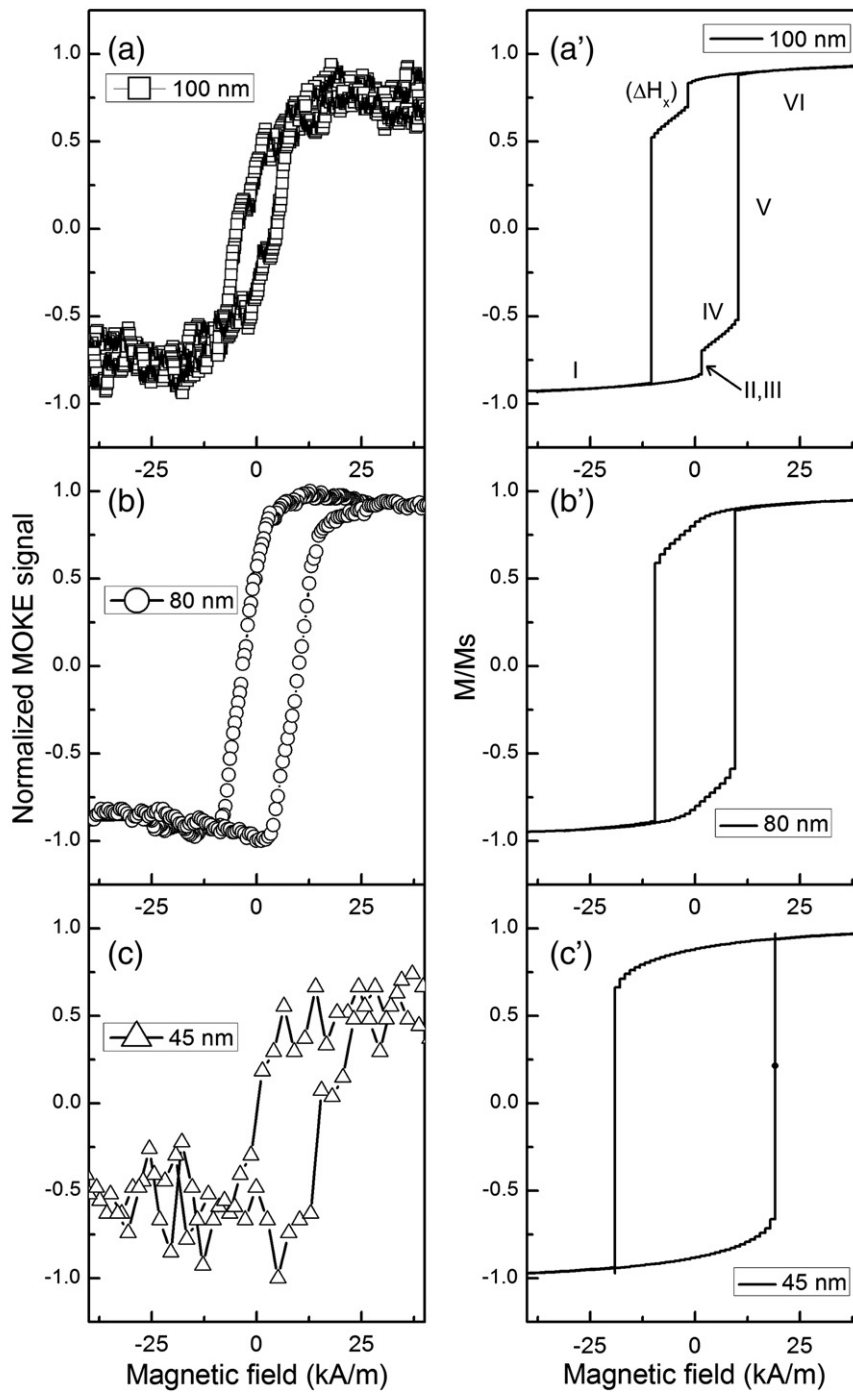


**Fig. 3.** The measured (a) and simulated (b) hysteresis loops of the triangular shaped dot arrays with lateral dimensions of 45 nm, 80 nm and 100 nm. The field is applied along the base direction of the triangles. The measured coercivities are 16 kA/m, 9.6 kA/m, and 9 kA/m, respectively.

resulting in a rectangular loop which is also in accordance with our measurements. These single switching loops reveal that there are no metastable states during the switching process. Thus, the reversal mechanism of the 45 nm and 80 nm triangles is dominated by the coherent rotation process. The simulated coercivity and saturation field are relatively larger than the measured values, possibly because the thermal fluctuation factors are not taken into considerations in the micromagnetic simulations, resulting in overestimated switching fields.

To aid our understanding of the spin reversal process in the nanotriangle, the simulated spin configurations are extracted. Shown in Fig. 4 are the spin states for the nanotriangle with  $L=100$  nm, where the corresponding conditions are marked in the hysteresis loop. When the field is reduced from negative saturation, the spins

near the edge of the triangles begin to deviate from the field direction, with a tendency to align along the edges (I). On reversing the magnetic fields to the positive direction, the spins located close to the bottom of the triangle remain unswitched. However, the spins located at the top corner rotate towards the perpendicular direction of the field. Consequently, a symmetric V-like spin configuration forms in the nanotriangle with the opening of the V opposite to the field direction (II). By increasing the field along the positive direction, the center of the V state sweeps towards the bottom (III). These processes cause the first switch in the hysteresis loop. Further increasing the field in the positive direction, a plateau extending 8 kA/m was observed in the simulated hysteresis loop. A relatively stable state was observed with top corner spins aligning perpendicular to the field direction, while those of

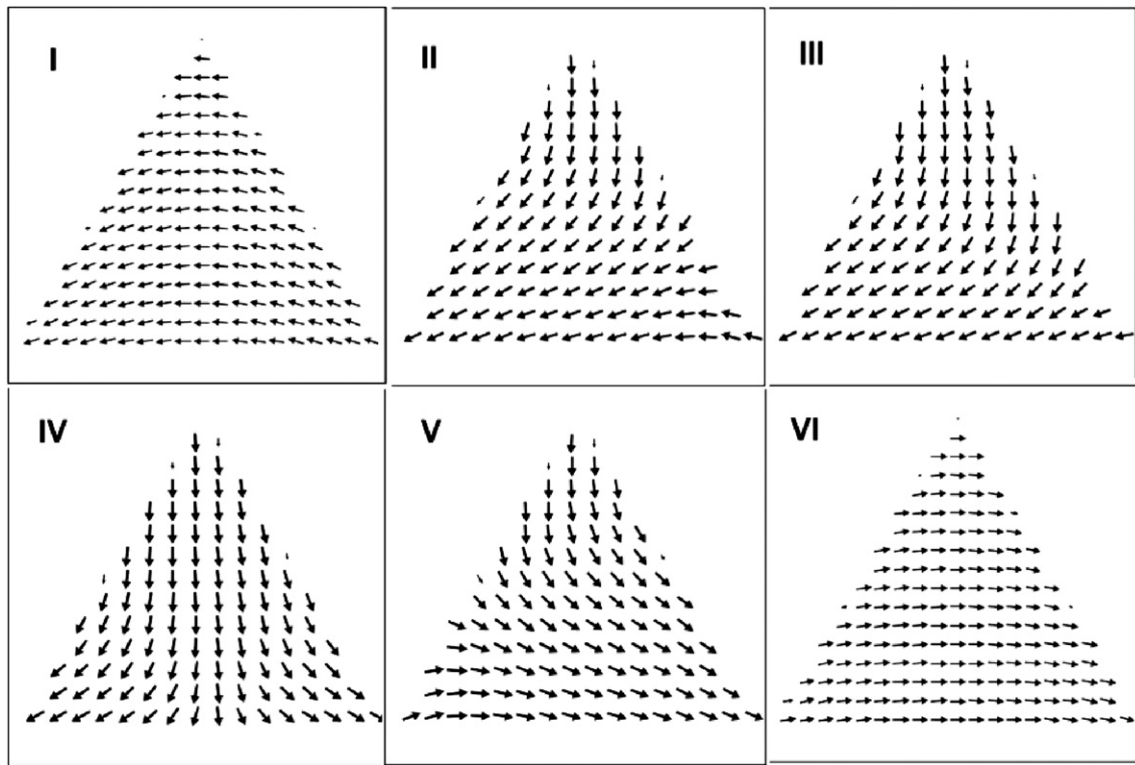


Fig. 4. The simulated magnetic configurations of the triangles. Corresponding applied fields are labeled on the simulated hysteresis loop in Fig. 2(b).

bottom base aligning along the field direction, forming a V state with the opening at the bottom (IV). As the field is increased to positive saturation, the spins in the nano-triangle begins to rotate towards the field direction, resulting in the second switch in the hysteresis loop. The spin configuration was a reversed V state (V). When the field is increased to a large positive value, the spin configuration reaches a positive saturation state (VI).

MFM imaging was carried out to observe the magnetic states of the triangular nanomagnets. MFM measurement on the 100 nm triangle was performed. A lift scan height of 50 nm was used for the scanning. Before scanning, the sample was magnetically saturated by applying a field of +120 kA/m along the major axis, the field was then reduced to 0 kA/m. Shown in Fig. 5 is the MFM image of the remanent state of the 100 nm triangular nanomagnets. The dark areas around the edges of the nanotriangles represent the pointy sides of

the V state. The V state is only found in some of the nanotriangles due to the fact that the nanotriangles are not aligned in one direction.

#### 4. Conclusions

In summary, arrays of sub-100 nm NiFe nanoscale triangle were fabricated by using nanosphere lithography techniques and their properties were characterized by MOKE magnetometry. MOKE measurements show that with the decrease of the lateral dimension of the triangle, the coercivity is increased. Micromagnetic simulations show that the reversal mechanism of the 45 and 80 nm triangles is dominated by the coherent rotation process, while that in the 100 nm triangle is via the formation and rotation of an intermediate V-like state.

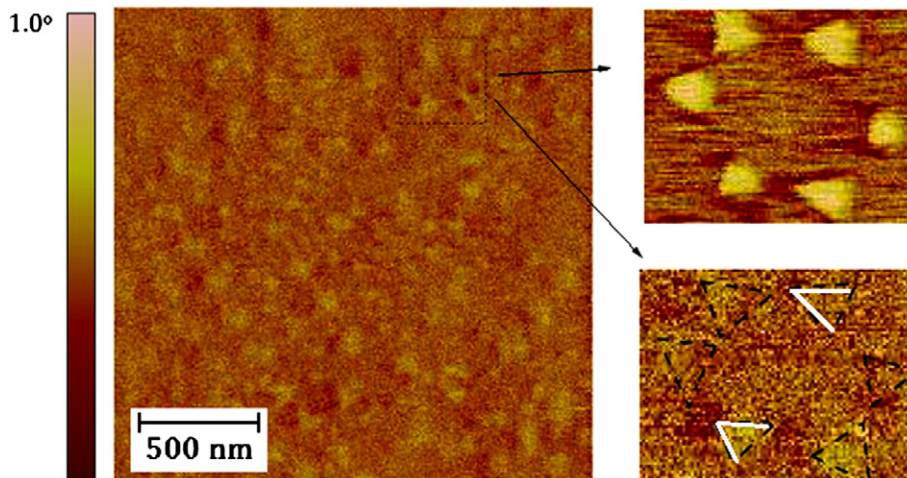


Fig. 5. MFM image of an array of triangular shaped NiFe nanomagnets. Inset is a close observation of a group of nanotriangles with schematic drawing to show the V state.

## Acknowledgments

This work was supported in part by the NRF-CRP program (Multifunctional Spintronic Materials and Devices) and the Agency for Science, Technology and Research (A\*STAR) SERC grant (082 101 0015).

## References

- [1] C.A.F. Vaz, J.A.C. Bland, G. Lauhoff, Rep. Prog. Phys. 71 (2008) 056501.
- [2] A. Wachowiak, J. Wiebe, M. Bode, O. Pietzsch, M. Morgenstern, R. Wiesendanger, Science 298 (2002) 577.
- [3] E. Saitoh, H. Miyajima, T. Yamaoka, G. Tatara, Nature 432 (2004) 203.
- [4] T. Shinjo, T. Okuno, R. Hassdorf, K. Shigeto, T. Ono, Science 289 (2000) 930.
- [5] M. Jaafar, R. Yanes, A. Asenjo, O. Chubykalo-Fesenko, M. Vazquez, E.M. Gonzalez, J.L. Vicent, Nanotechnology 19 (2008) 285717.
- [6] S.P. Li, D. Peyrade, M. Natali, A. Lebib, Y. Chen, U. Ebels, L.D. Buda, K. Ounadjela, Phys. Rev. Lett. 86 (2001) 1102.
- [7] R.P. Cowburn, D.K. Koltsov, A.O. Adeyeye, M.E. Welland, D.M. Tricker, Phys. Rev. Lett. 83 (1999) 1042.
- [8] C.A. Ross, M. Hwang, M. Shima, J.Y. Cheng, M. Farhoud, T.A. Savas, Henry I. Smith, W. Schwarzacher, F.M. Ross, M. Redjail, F.B. Humphrey, Phys. Rev. B 65 (2002) 144417.
- [9] J. Aizpurua, P. Hanarp, D.S. Sutherland, M. Kall, G.W. Bryant, F.J.G. de Abajo, Phys. Rev. Lett. 90 (2003) 057401.
- [10] J. Rybczynski, U. Ebels, M. Giersig, Colloids Surf., A 219 (2003) 1.
- [11] Y. Yin, Y. Lu, B. Gates, Y. Xia, Chem. Mater. 13 (2001) 1146.
- [12] M. Trau, D.A. Saville, I.A. Aksay, Science 272 (1996) 706.
- [13] F.Q. Zhu, G.W. Chern, O. Tchernyshyov, X.C. Zhu, J.G. Zhu, C.L. Chien, Phys. Rev. Lett. 96 (2006) 27205.
- [14] M.J. Donahue, D.G. Porter, OOMMF User's Guide, Version 1.0, Interagency Report NISTIR 6376, National Institute of Standards and Technology, Gaithersburg, MD, 1999.